eprints@whiterose.ac.uk
https://eprints.whiterose.ac.uk/

Extremely large d^0 magnetism in krypton implanted polar ZnO films

Minju Ying[1,2*], Ahmad M.A. Saeedi[3], Miaomiao Yuan[1], Xia Zhang[1], Bin Liao[1], Xu Zhang[1], Zengxia Mei[4], Xiaolong Du[4], Steve M Heald[5], A. Mark Fox[3], Gillian A. Gehring[3*]

1 Key Laboratory of Beam Technology of Ministry of Education, College of Nuclear Science and Technology, Beijing Normal University, Beijing 100875, China
2 Beijing Radiation Center, Beijing 100875, China
3 Department of Physics and Astronomy, Hicks Building, University of Sheffield, Sheffield S3 7RH, United Kingdom
4 Beijing National Laboratory for Condensed Matter Physics, Institute of Physics, Chinese Academy of Sciences, Beijing 100190, P. R. China
5 Advanced Photon Source, Argonne National Laboratory, Argonne, IL 60439, United States of America

[*]Authors to whom correspondence should be addressed
  Electronic addresses: mjying@bnu.edu.cn and g.gehring@sheffield.ac.uk

Abstract

Magnetization is produced in samples of ZnO by implanting krypton ions. Krypton is chemically inert hence the magnetization is the consequence of the radiation damage that occurred due to the implantation process. We have found magnetizations as large as 185 emu/cm^3 at room temperature which corresponds to a moments of ~40 Bohr magnetons per implanted krypton ion. Results are compared for implantation into different ZnO samples, O and Zn polar thin films and thin ZnO crystal wafers. The structure of the films has been investigated using RHEED, AFM, XRD and EXAFS. The O-polar film grew in a layer-by-layer mode and after implantation, its lattice spacing increased and the grain size decreased which indicated that the Kr atoms had been incorporated into the lattice. In contrast the Zn-polar film grew in Stranski-Krastanov mode and its lattice spacing and grain size were almost unchanged by the implantation indicating that the Kr atoms were in the grain boundaries. Raman scattering is used to characterize the radiation damage and to identify scattering from amorphous regions in grain boundaries and the scattering from point defects. The largest magnetization is found in the O-polar ZnO films where there is a marked grain fragmentation, leading to an increase in the volume of the sample occupied by grain boundaries. The increase in the numbers of point defects, which were identified by Raman scattering for films of both polarity, was less effective at producing a magnetic signal than the grain boundaries.

1. Introduction

ZnO-based dilute magnetic semiconductors (DMS) have attracted much attention over the past decade for potential application in spintronic devices [1-3]. Many papers report that the inclusion of transition metal (TM) dopants in ZnO leads to room temperature (RT) ferromagnetism [2,3]. Magnetism has also been observed in non-TM or un-doped ZnO, this is a new area of research, defect induced ferromagnetism, or d^0 ferromagnetism [4-8]. ZnO is nonmagnetic when it is stoichiometric and its conductivity is very low. It has been shown to exhibit d^0 magnetization when it has been grown with a large excess of oxygen and this has been attributed to Zn vacancies which are acceptors [9-11] but it is also magnetic when it is grown oxygen deficient and then the magnetization is attributed to oxygen vacancies and the conductivity is n-type [12-14]. Coey et al. proposed that the magnetism is due to a shallow impurity band that could split spontaneously, if it was sufficiently narrow, and that the temperature dependence of the magnetization would be as described by Stoner theory leading to a very high transition temperature [15, 16]. Some authors have considered that this impurity band arises from point defects [8] but others have argued that it originates at grain boundaries [17-19]. Our results point clearly to the importance to magnetism of the grain boundaries in our samples of ZnO.

Ion implantation is a non-equilibrium and reproducible method to introduce defects into crystalline materials. Accelerated ions will leave a trail of atoms displaced from their equilibrium lattice sites, thus creating vacancies, interstitials or antisites which both donors and acceptors [20] before they finally come to rest. The distribution and concentration of the defects can be controlled by varying the ions energy and dose.

ZnO has the wurtzite structure with a lack of inversion symmetry along the c-axis so that ZnO has opposite polarization faces along this direction which are Zn-polar ZnO(0001) and O-polar ZnO($000\bar{1}$). The two polar surfaces are reported to give structurally and chemically different films [21]. The surface porosity and ability to absorb impurities of the O-polar films has led to their use in catalysis [22-24]. Our previous work showed that magnetism was observed for As implanted in O-polar, but was very weak in Zn–polar films [25]. Arsenic is a group five element that has been considered as a candidate for hole doping in ZnO due to the formation of a magnetic (As_{Zn}-$2Zn_v$) complex [26]. This work describes the magnetic effects of defects produced solely by radiation damage and not by chemical bonding as the Kr atom is inert. We report on a series of experiments of implantation of 300 nm thick polar ZnO films that were grown on sapphire substrates using a radio frequency plasma-assisted molecular

beam epitaxy (MBE) system and also on commercially sourced polar ZnO single crystals with thickness of 0.5mm. The polar crystals have one O-polar and one Zn –polar face and both faces were implanted and studied in what follows.

2. Experimental details

A RF plasma-assisted MBE system (OmniVac) was used to grow high quality O and Zn polar ZnO films of 300nm on sapphire substrates. Sapphire substrates were exposed to an oxygen plasma (270W/1.5sccm) at 500 ℃ for 30 mins to obtain a uniform oxygen-terminated surface [27]. After that, a thin MgO buffer layer was prepared at 500 ℃, which was followed by a ZnO buffer layer and an epilayer growth at 450℃ and 650 ℃ respectively. It was found that an ultrathin rocksalt-MgO buffer layer leads to O polar ZnO while a thick wurtzite-MgO results in Zn polar ZnO [27]. The in-plane epitaxial relationship and surface morphology evolution were monitored in situ by reflection high-energy electron diffraction (RHEED). Kr ions were also implanted into commercial ZnO wafers that were 0.5mm thick. These wafers been prepared with O-polar and Zn-polar surfaces by Hefei Kejing Materials Technology CO., LTD . High quality krypton ions were introduced into the O-polar and Zn-polar ZnO films and wafers by using ion implantation. A sequence of four implantation energies (200KeV, 150KeV, 80KeV, and 30KeV) was used to produce a nearly even distribution of Kr ions throughout a thickness of about 70 nm in the samples. Three concentrations of 5×10^{19}, 1×10^{20}, and 5×10^{20} cm^{-3} for Kr ions were implanted and studied in this paper. X ray diffraction (XRD) and Raman spectroscopy measurements have been carried out to characterize the implantation induced disorder in ZnO films and crystals. The position of the Kr in the lattice was observed directly using extended x-ray absorption fine structure spectroscopy (EXAFS) taken at beamline 20-BM at the Advanced Photon Source using fluorescence detection with a 13-element Ge detector and a Si (111) monochromator. Atomic force microscopy (AFM) was used to show the evolution of the surface morphology of polar ZnO films after implantation. The magnetic properties were characterized using a superconducting quantum interference device (SQUID) magnetometer. The magnetization of the Kr doped films was found by subtracting the signal measured for the undoped ZnO films on the substrate from that obtained for the implanted film.

3. Results and discussion

Figures 1 (a) and (b) show the RHEED patterns during the growth of O polar and Zn polar ZnO films on Al$_2$O$_3$(0001) substrates, taken along the [10$\bar{1}$0] azimuth of sapphire substrate.

An ultrathin rocksalt-MgO buffer (<1 nm) layer leads to O polar ZnO with very flat surface morphology and grown in a layer-by-layer mode, as is confirmed by the sharp streaky RHEED pattern in Fig. 1(a) for ZnO epilayer. A thick wurtzite-MgO results in Zn polar ZnO, which is grown in a typical Stranski-Krastanov mode. The in-plane epitaxial relationship for polar ZnO films are ZnO $[11\bar{2}0]$ //Al$_2$O$_3$ $[10\bar{1}0]$ and ZnO $[11\bar{2}0]$ //MgO $[11\bar{2}0]$ //Al$_2$O$_3$ $[10\bar{1}0]$, respectively.
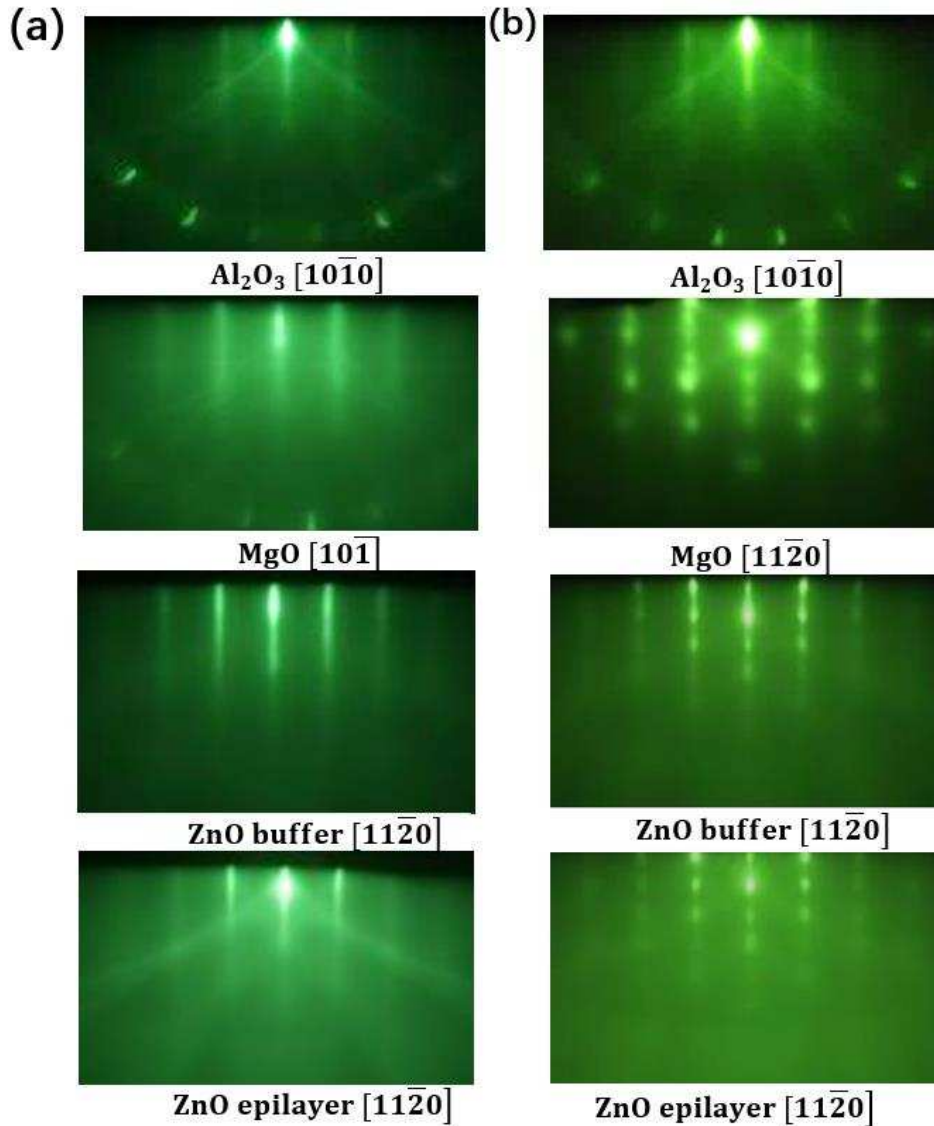

Fig.1 The RHEED pattern evolution during the growth of O polar (a) and Zn polar (b) ZnO films on Al₂O₃(0001) substrates, taken along the $[10\bar{1}0]$ azimuth of sapphire substrate.

The Kr ions were implanted at sequences of four implantation energies (200KeV, 150KeV, 80KeV, and 30KeV) so as to produce a nearly even distributions of Kr ions throughout ~70nm of the films, the dose at each energy is given in Table 1. The implantation dose was chosen to give concentrations of $5\times10^{19}/cm^3$, $1\times10^{20}/cm^3$ and $5\times10^{20}/cm^3$ in a range $10<x<70$ nm from the surface of the sample as indicated in figure 2.

Table 1 The implantation parameters: energies, doses and concentrations

Energies	Dose（Φ）	Concentration of Kr at chosen depth
200KeV, 150KeV, 80KeV, 30KeV	2.5×10^{14} cm^{-2}, 5×10^{13}cm^{-2}, 7.5×10^{13} cm^{-2}, 5×10^{13} cm^{-2}	5×10^{19}cm^{-3}
200KeV, 150KeV, 80KeV, 30KeV	5×10^{14}cm^{-2}, 1×10^{14}cm^{-2}, 1.5×10^{14}cm^{-2}, 1×10^{14}cm^{-2}	1×10^{20}cm^{-3}
200KeV, 150KeV, 80KeV, 30KeV	2.5×10^{15}cm^{-2}, 5×10^{14}cm^{-2}, 7.5×10^{14}cm^{-2}, 5×10^{14}cm^{-2}	5×10^{20}cm^{-3}
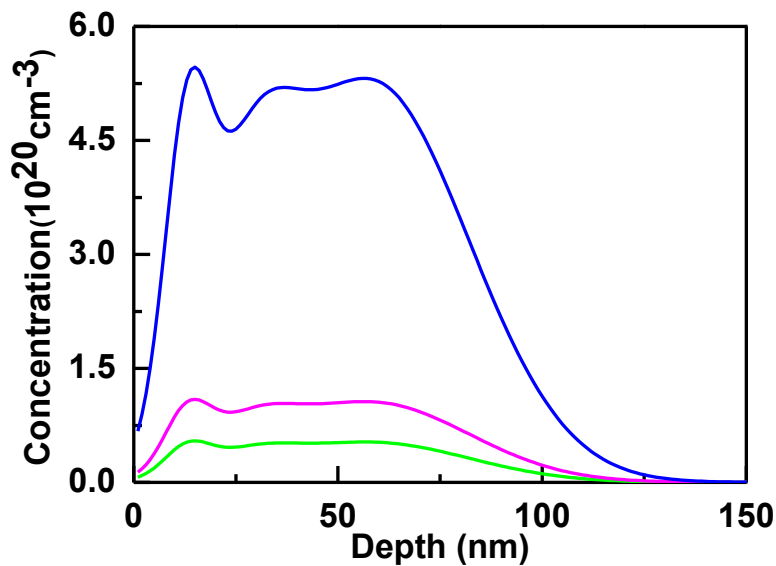
FIG. 2 (color online) The summed implants distribution profiles of Kr ions; showing quasi uniform concentrations of $5\times10^{19}/cm^3$,$1\times10^{20}/cm^3$, and $5\times10^{20}/cm^3$ at depths $10<d<70$nm. (Implanted using sequence of four implantation energies.)

XRD patterns were obtained from the undoped and Kr implanted polar ZnO films and crystals in θ-2θ geometry. All the samples exhibit a single phase with a typical wurtzite structure with only ZnO (0002) and (0004) diffraction peaks observed demonstrating that the c-axis was oriented out of plane. The diffraction peaks from the sapphire substrate, marked as S were observed but no secondary phases were detected when the data was examined on a log scale. Fig. 3(a) shows the XRD patterns for the Kr doped O-polar ZnO films. The enlarged ZnO (0002) peaks is shown in Fig.3 (b) which illustrate that the diffraction peaks shift towards lower angle with an increase of doping concentration for Kr doped O polar films, demonstrating that the c lattice parameter undergoes an obvious expansion after implantation. The lattice parameters and the full width of half maximum (FWHM) of ZnO(0002) are given in Table II for the O and Zn polar films and both faces of the wafers obtained from XRD. The increase of FWHM with implantation is an indication of grain fragmentation because of the large lattice expansion caused by Kr incorporation. The O-polar films show the largest increase of FWHM and grain fragmentation after Kr doping larger than 5×10^{19}cm^{-3}. The grain sizes after Kr implantation were estimated for the polar films. As it is not valid to calculate the grain size by the Scherrer formula when the value is larger than 100 nm, we did not give the results for the undoped films and all the wafers, as they are all greater than 100 nm from Scherrer formula calculation. The large lattice expansion and small grain size in the Kr doped O polar films imply that a large fraction of the implanted Kr atoms go into the grains for O polar films. Their absence for the Zn-polar films show that the majority of Kr is located in the grain boundaries for Zn polar films. It is possible that the large lattice expansion has caused the fragmentation of some grains so the average grain size is reduced. The island surface structure, as is evidenced by RHEED, observed for the Zn polar film that cause the implanted Kr ions go into the grain boundary. The AFM images shown in Fig. 4 also confirm the flat surface morphology of undoped O polar ZnO and the island structure for Zn polar film. An obvious granulation of O polar films is observed with the increase of the Kr concentration. Relative small changes were observed for the Zn polar ZnO after implantation which was consistent with our observation that the Kr ions were in the grain boundaries in Zn polar films.
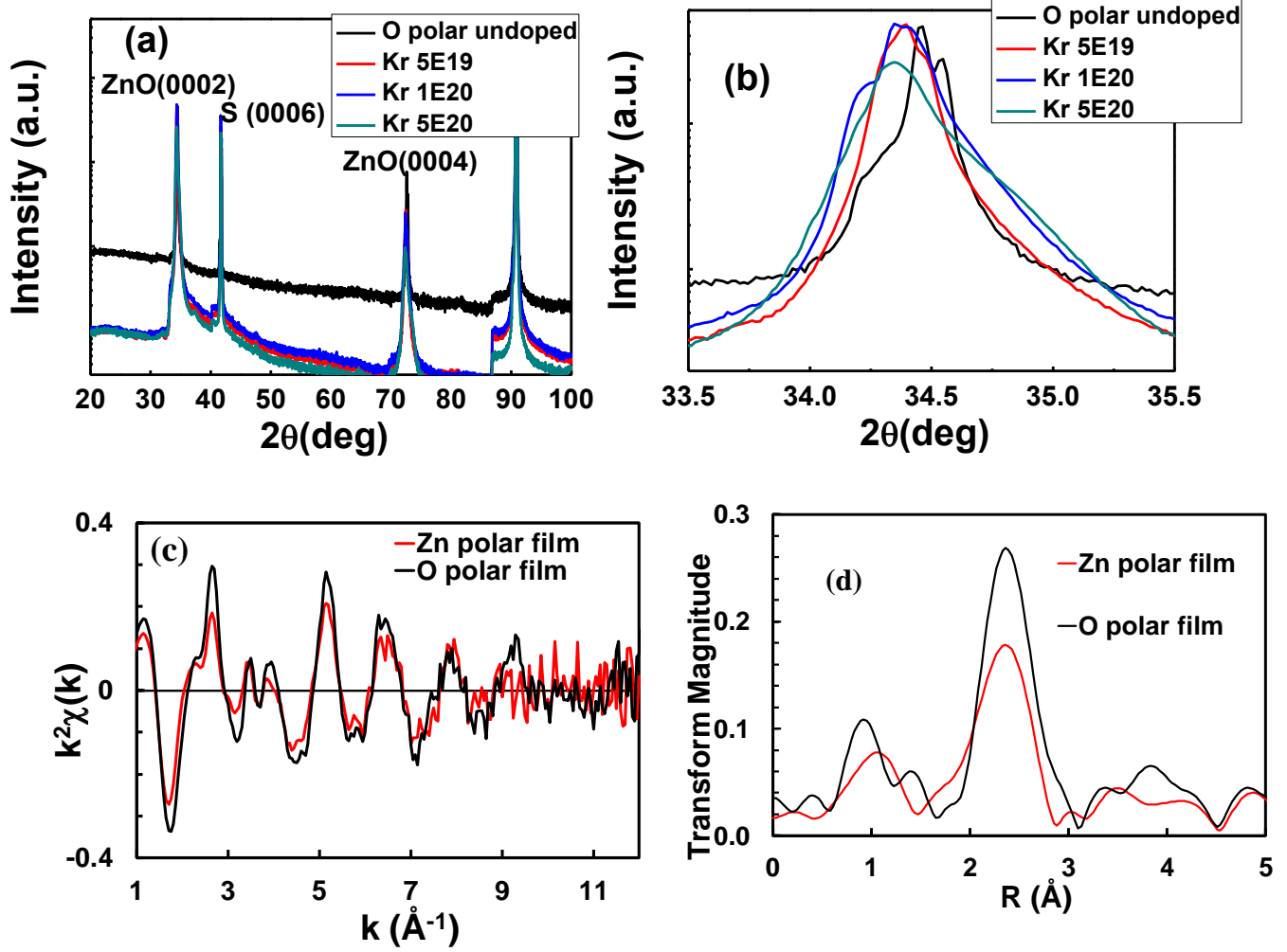
FIG. 3 (color online) (a) and (b) the XRD data for the O-polar film showing (a) all reflections (the XRD peaks marked as S are from the Al_2O_3 substrate) and (b) an enlarged plot of the ZnO(0002) reflection (using a log scale) (c) and (d) EXAFS data for 5×10^{20} cm^{-3} Kr doped O polar and Zn polar ZnO films; (c) a plot of $\kappa^2 \chi(\kappa)$ and (d) $|\chi(R)|$

Table Ⅱ The calculated lattice constants, FWHMs and grain sizes for the ZnO films and wafers.

Samples	Lattice constant (±0.002Å)				FWHM(±0.005Degree)/Grain size (±5nm)			
	undoped	5×10^{19}	1×10^{20}	5×10^{20}	undoped	5×10^{19}	1×10^{20}	5×10^{20}
Doped O polar films	5.202	5.211	5.214	5.222	0.0710	0.0915/ 90	0.1113/ 74	0.1497/ 55
Doped	5.202	5.203	5.203	5.205	0.0634	0.0800/	0.0850/	0.0905/

Zn polar films						>100	97	91
Doped O polar wafers	5.205	5.207	5.208	5.207	0.0634	0.0824	0.0832	0.0778
Doped Zn polar wafers	5.205	5.207	5.208	5.208	0.0659	0.0687	0.0785	0.0778

(a)   O polar film   **(b)   Zn polar film**
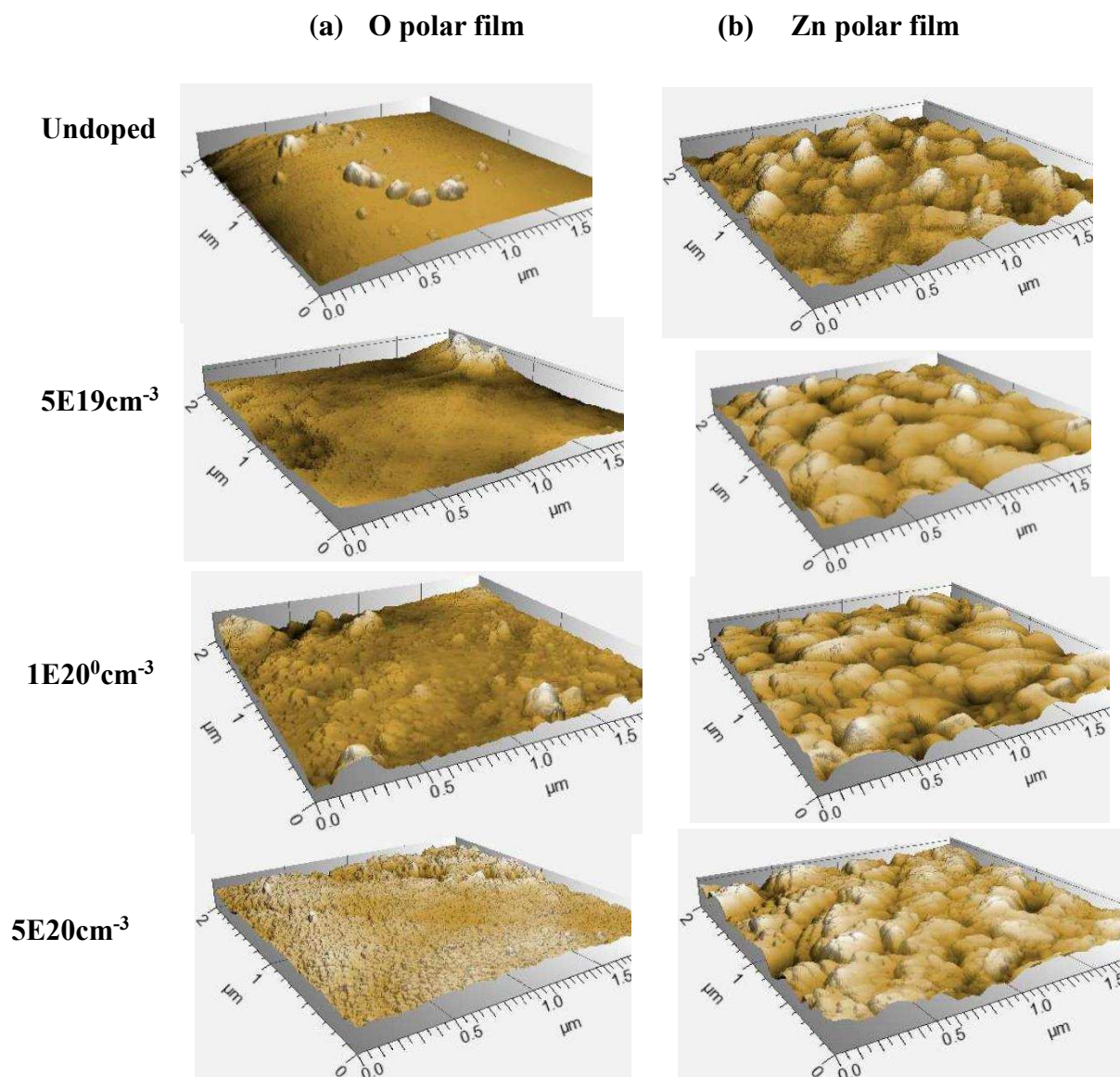
Fig. 4 The evolution of surface morphology shown by AFM for O polar (a) and Zn polar (b) ZnO films in 2 ㎛×2 ㎛, with Kr concentration from zero (undoped) to $5×10^{20}$ cm^{-3}.

The position of the Kr in the lattice was observed directly using EXAFS data shown in

Fig. 3 (c) and (d). This data was taken at beamline 20-BM at the Advanced Photon Source using fluorescence detection with a 13-element Ge detector and a Si (111) monochromator. Data collected in two separate runs were consistent, and the Fig. 3(c) shows the summed data from these runs. The EXAFS from both samples was very weak indicating the Kr atoms are in disordered sites.The small EXAFS amplitude made accurate background subtraction important.Kr has strong multi-electron features in the background that were removed by subtracting the background determined from Kr gas. The gas has the multi-electron background, but no EXAFS. The low R features in the transforms are the residuals of this background. There is a clear difference with the Zn polar sample having a smaller amplitude, which means more disorder and/or fewer neighbors in Zn polar samples. This is consistent with our XRD results that show the Kr atoms go to the grain boundary for the Zn polar films and into the grains for O polar film, resulting in a more disorder and/or few neighbors in Zn polar ZnO. Measurements were also taken of the Zn near edge absorption. Obviously, this measured all the Zn atoms in the film including those in the un-implanted region. There was no significant difference observed when the doped O polar film was compared with the doped Zn polar film (the data is shown as additional material). This indicates that we have no clear evidence that the defects that were formed increased or decreased the Zn ionization although the presence of the magnetism certainly implies that the implanted film has charged defects.

Raman scattering was used to identify the density of grain boundaries and point defects are measured by in $z(xx)\bar{z}$ geometry using 514.5 nm laser excitation. Since the films were thin the sapphire peaks, labelled 'S' at 380 cm^{-1}, 418 cm^{-1}, 578 cm^{-1} and 752 cm^{-1}, are dominant in Fig.5. For the undoped film, there are only two ZnO peaks, labeled with E_2(L) at 101 cm^{-1} and E_2(H) at 439 cm^{-1}. The low-frequency E_2 mode is associated with the vibration of the heavy Zn sublattice, while the high-frequency E_2 mode involves the oxygen sublattice [28] and the absence of other peaks in the spectra from the pure films show that there were no secondary phases within the detection limit.

The total Raman intensity increased greatly in the implanted films. A new strong peak emerged at 580 cm^{-1} with a possible shoulder on the low frequency side as has been seen previously in doped and implanted ZnO [25,28-31] but also a strong broad response between 50 cm^{-1} and 300cm^{-1} and a signal that increased, approximately linearly from 300 cm^{-1} to 500cm^{-1}. The peak at 580 cm^{-1} also appears in studies of nanoparticles [32,33] and may be related to the two Raman signals A_1(LO) at 584 cm^{-1} and E_1(LO) at 595 cm^{-1} that were forbidden for the pure films in $z(xx)\bar{z}$ geometry. The broadening around 540 cm^{-1} is attributed to multi-phonon scattering due to defects. The response between 50 cm^{-1} and 300 cm^{-1} follows

the phonon density of states [34,35] and is attributed to the amorphous regions in the domain walls. A similar signal was also seen for As implanted ZnO [25] but not for nanoparticles [32] implying that it is the region of the grain boundary itself rather the finite grain size that is giving rise to this signal.

The signals from pure ZnO seen at 101 cm^{-1} and 438 cm^{-1} are still clearly visible in Fig. 3(b) for the Zn–polar film but significantly weakened and broadened in Fig. 4(a) for the O-polar film. The peak at 438 cm^{-1} is clearly visible in other implanted ZnO films and doped nanoparticles [22,29,33]. This demonstrates that O-polar films are especially prone to become damaged. The low energy scattering dominates the signal from the O-polar film that was found to have reduced grain size. The peak at ~580 cm^{-1} is significantly stronger for the Zn-polar film which implies more numerous point defects in that film although the overall crystallinity that has been preserved so that the Raman lines $E_2(L)$ and $E_2(H)$ remain visible.
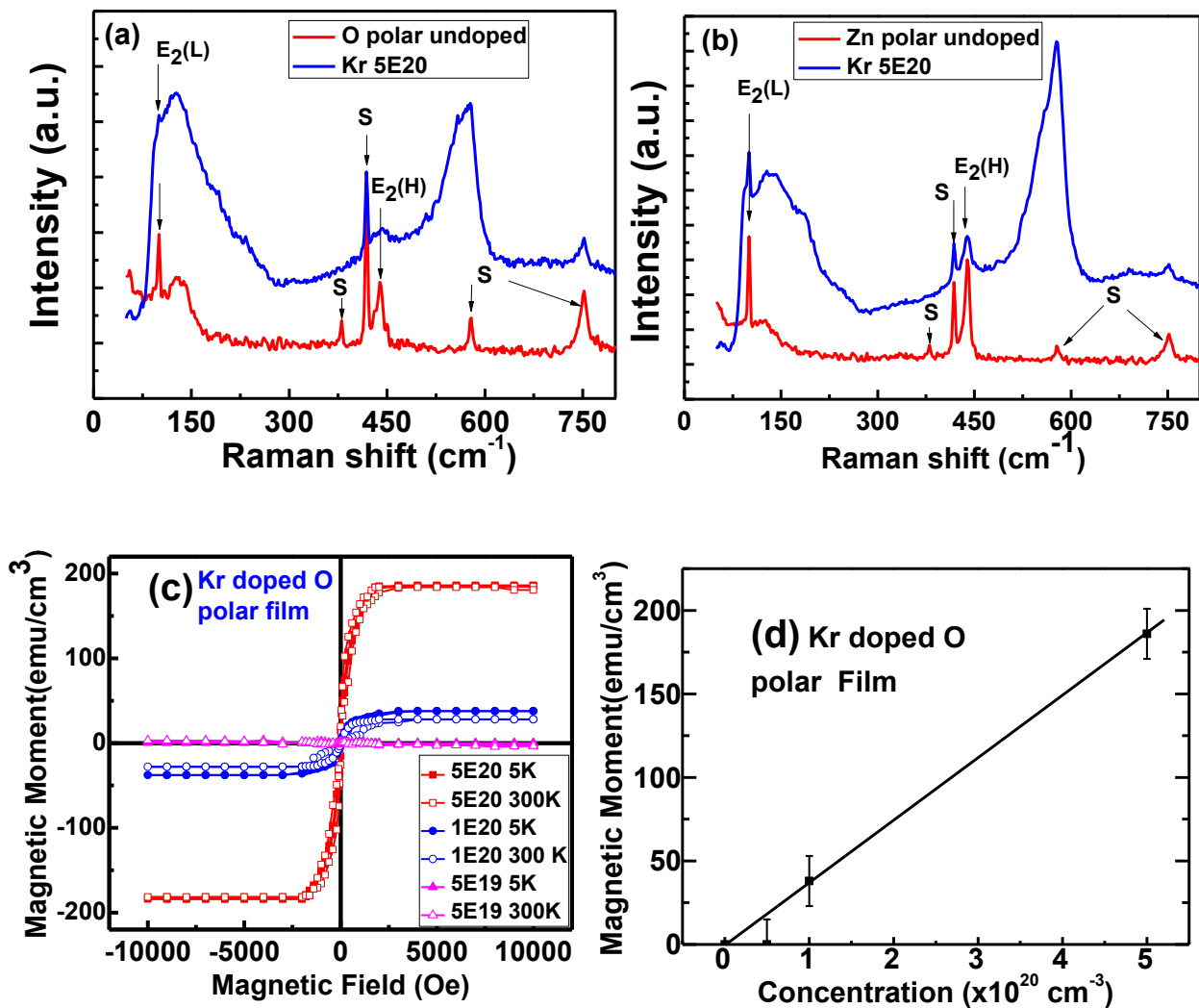

Fig. 5 (color online) Raman spectra for the undoped (red) and 5×10^{20} cm^{-3} Kr doped (blue) ZnO films. (a) O polar (b) Zn polar films and (c) M-H loops for the O-polar film

for Kr concentrations of 5×10^{19} cm^{-3}, 1×10^{20} cm^{-3} and 5×10^{20} cm^{-3} measured at 300K and 5K (d) Magnetization of the O-polar film measured at 5K as a function of Kr concentration. (The magnetization was assumed to arise from the optimally implanted region 10<d<70nm as shown in Figure 2)

Magnetism measurements were performed for both doped and undoped samples at 5 K and 300 K. Exceptionally large magnetic moments were observed in the O-polar films but no magnetic moments at all were detected in either the Zn-polar films or in the crystal when either of its faces were implanted with Kr.

Figure 5(c) shows the field dependence of magnetization (M-H) curves, which were taken at 5K and 300K on the undoped and Kr doped O polar ZnO films. The signal from an undoped ZnO film on a substrate has been subtracted from these plots and this has introduced an error of ±10 emu into all our measurements. No magnetization, at either temperature, was observed for the 5×10^{19} cm^{-3} Kr doped ZnO films but when the Kr doping concentration was increased to 1×10^{20} cm^{-3}, obvious magnetic hysteresis loops have been observed with a saturation magnetization of 38 and 28 emu/cm^{3} at 5 K and 300 K, respectively. When the doping concentration is further increased to 5×10^{20} cm^{-3}, very substantial temperature-independent ferromagnetism has been observed with the saturation magnetization of 186 and 185 emu cm^{-3} at 5 K and 300 K, respectively.

The dependence of the magnetization on the Kr concentration is shown in Fig.4(d), which shows that the magnetization is nearly linear with Kr concentration. The saturation magnetism, Ms, and the moment per implanted Kr for the O-polar films at 5 K and 300 K are shown in Table III. The very large moment observed per Kr ion indicates that it has occurred during the implantation process rather than being associated with a local moment from the Kr substituted in the ZnO lattice. The lack of any observable temperature dependence of the magnetization for the most heavily doped film and low coercive field is characteristic of magnetization due to defects [15,18,36]. The film doped with 1×10^{20} cm^{-3} Kr ions had the same moment associated with each ion but in this case the coupling between the magnetizations in different defective regions is weaker leading to a reduced magnetization at 300K. The grain sizes of these films, 55nm for 5×10^{20} cm^{-3} and 74nm for the 1×10^{20} cm^{-3} doped films respectively, are both rather larger than the critical value of ~33 nm proposed earlier [19]. The moment per Kr is significantly larger than that deduced for implanted As which was 27μ_B/As [25].

We have also introduced an alternative method for calculating the moment per Kr atom

whereby we calculate the total number of Kr atoms in our films using the doses given in Table I. The moment per Kr calculated from this value is significantly lower since it is assumed to be shared by all the Kr atoms and not just the ones in the region of highest density. This alternative value is $28\mu_B$/Kr which is still very much higher than might be expected to originate from a defect state localized at the Kr.

Table III The saturation magnetism, Ms, and the moment per implanted Kr for O polar ZnO films at 5K and 300K.

O polar film	Ms (emu/cm^3)		Ms (μ_B/Kr)	
	5 K	300 K	5 K	300 K
undoped	0	0	0	0
5×10^{19} cm^{-3}	0 ± 10	0 ± 10	0 ± 20	0 ± 20
1×10^{20} cm^{-3}	38 ± 10	28 ± 10	41 ± 10	30 ± 10
5×10^{20} cm^{-3}	186 ± 10	185 ± 10	40 ± 2	40 ± 2

We have shown that the structural properties of the implanted O-polar ZnO film are distinct from those of the Zn-polar film and the ZnO wafer. This was shown by the XRD and EXAFS that showed that the Kr was incorporated into the lattice rather than a grain boundary and the grain size decreased most dramatically for the O-polar film. The Raman spectra showed that the grain boundaries were scattering strongly for the O-polar film. By contrast there was stronger evidence of point defect scattering from the Zn-polar film which was not magnetic. We believe that the well-known tendency of the O-polar films to absorb impurities [22-24] and its flat surface morphology has led to the incorporation of the Kr ions in the lattice and the large size of the Kr relative to zinc or oxygen has led to the strains that cause the grains to fracture and produce the grain boundaries that are responsible for the magnetism.

The observed magnetization was almost independent of temperature implying that it arises from polarized electrons in a narrow defect band [16]. Thus we expect that the magnetism arises from those defects that are sufficiently close to each other to form defect bands; other deep isolated defects that have localized states will not play an important role. We can also expect that both donor and acceptor defects are formed as, for example a Zn vacancy (acceptor) and a Zn interstitial (donor) are formed.

Grain boundaries are regions where there are complex defects. A grain-boundary defect

model has been proposed which suggests that the negative charged Zn vacancies reside on the grain boundary to compensate the positively charged O vacancies extending into the adjacent grains [37]. Positron annihilation spectroscopy (PAS) has been performed in a Doppler mode to characterize the negatively charged grain-boundary defect, V_{Zn} at the grain-boundary interface in ZnO [38]. Recent theoretical study on d^0 magnetism in ZnO also show that the Zn vacancy tends to be attracted more easily to the grain boundaries relative to the bulk-like region and V_{Zn} induces spin polarization to the O sites originating from the O 2p orbitals at the grain boundary [39].

In our experiment, implanted Kr ions go into the grains for O polar ZnO and introduce various vacancies and interstitials and a marked grain fragmentation. The Zn vacancies may be attracted to the grain boundary and form the defects bands which are magnetic. In this work, we used Raman spectra to study the defects. Point defect can give Raman scattering at high wave vector, while complex defects at the grain boundary are large so can give a response at low wave vector. The low energy scattering dominates the signal from the O-polar film that was high magnetic, while the peak at ~580 cm^{-1} is significantly stronger for the Zn-polar film which implies more numerous point defects in that film. Our work has indicated that ion implanted O-polar ZnO films are particularly prone to generate amorphous regions that are strongly magnetic.

Our work has also shown that the magnetism in the boundary region at the surface of grains depends on how this surface is generated. The surface of nano-particles generates almost no magnetism and the Raman spectrum from nano-particles is very different from that found from the implanted crystals [32]. We have shown that the grain boundaries that are produced due to ion implantation are more efficient at generating magnetism than those that have been observed previously [17-19] and that ion implanted O-polar ZnO films are particularly prone to generate amorphous regions that are strongly magnetic.

4. Conclusions

In this paper, multi-energy ion implantation has been employed to introduce different concentrations of krypton into different systems, O and Zn polar thin films and a thin ZnO crystal wafer. We have shown by the XRD and EXAFS that the Kr was incorporated into the lattice rather than a grain boundary and the grain size decreased most dramatically for the O-polar film. The largest magnetization of 185 emu/cm^3 at room temperature that corresponds to a moment of ~40 Bohr magnetons per implanted krypton ion is found only in the O-polar ZnO

films. This is accompanied by a marked decrease in the grain size, as indicated by XRD, leading to an increase in the volume of the sample occupied by grain boundaries. In contrast, the increase in the numbers of point defects, which were identified by Raman scattering, were less effective at producing a magnetic signal. We have shown that the grain boundaries that are produced as a result of ion implantation are more efficient at generating magnetism than those that have been observed previously. Our work has indicated that ion implanted O-polar ZnO films are particularly prone to generate amorphous regions associated grain boundaries that are strongly magnetic.

Author contributions

M.Y, G.G and M.F wrote the main manuscript text, A.S performed the magnetic analysis, M.Y, X. Z, B.L and X.Z carried out the ion implantation and XRD, Raman and AFM measurements, Z. M, X.Du prepared the polar ZnO films by MBE, S.H carried out the X-ray absorption spectroscopy and analyzed the data. All the authors edited, discussed and approved the whole paper.

Conflicts of interest
There are no conflicts of interest to declare

Reference
[1] H. Ohno, Science 1998, **281**, 951.

[2] S. A. Wolf, D. D. Awschalom, R. A. Buhrman, J. M. Duaghton, S. von Molnar, M. L. Roukes, A. Y. Chtchelkanova, and D. M. Treger, Science 2001, **294**, 1488.

[3] T. Dietl, H. Ohno, F. Matsukura, J. Cibert, and D. Ferrand, Science 2000, **287**, 1019.

[4] T.K. Nath, A.J. Behan, J.R. Neal, D. Score, Q. Feng, A.M Fox, G.A. Gehring, J. Magn Magn. Mater. 2011, **323,** 1033.

[5] F. Pan, C.Song, X. J. Liu, Y. C Yang, F. Zeng,Mater. Sci. Eng., R 2008, **62**,1.

[6] C. Song, F. Zeng, K. W. Geng, X. J. Liu, F. Pan, B. He, W.S. Yan,Phys. Rev. B 2007, **76,** 045215.

[7] G. Z. Xing, J. B. Yi, J. G. Tao, T. Liu, L. M. Wong, Z. Zhang, G. P. Li, S. J. Wang, J. Ding, T. C. Sum, C. H. A. Huan, and T. Wu, Adv. Mater 2008, **20,** 3521.

[8] B. Qi, S. Ólafsson, H.P. Gíslason, Progress in Materials Science 2017, **90**, 45.

[9] Nguyen Hoa Hong, Joe Sakai and Virginie Briz´e, J. Phys.: Condens. Matter 2007, **19**, 036219.

[10] J. B. Yi, C. C. Lim, G. Z. Xing, H. M. Fan, L. H. Van, S. L. Huang, K. S. Yang, X. L. Huang, X. B. Qin,B.Y. Wang, T. Wu, L. Wang, H. T. Zhang, X.Y. Gao, T. Liu, A. T. S. Wee, Y. P. Feng, and J. Ding, Phys. Rev. Lett. 2010, **104**, 137201.

[11] G.Z. Xing, Y.H. Lu, Y.F. Tian, J.B. Yi, C.C. Lim, Y.F. Li, G.P. Li, D.D. Wang, B. Yao, J. Ding, Y.P. Feng, T. Wu, AIP Advances 2011, **1**, 022152.

[12] P. Zhan, W. Wang, C. Liu, Y.Hu, Z.C. Li, Z.J. Zhang, P. Zhang, B.Y. Wang, X.Z. Cao, J. Appl. Phys. 2012, **111**, 033501.

[13] P. Zhan, Z. Xie, Z.C. Li, W.P. Wang, Z.J. Zhang, Z.X. Li, G.D. Cheng, P. Zhang B.Y. Wang, X.Z. Cao, Appl. Phys. Lett. 2013, **102**, 071914.
[14] G.Z. Xing, D.D. Wang, J.B. Yi, L.L. Yang, M. Gao, M. He, J.H. Yang, J. Ding, T. C. Sum, T. Wu Appl. Phys. Lett. 2010, **96**, 112511.

[15] J.M.D. Coey, M. Venkatesan, C.B. Fitzgerald, Nature Mater. 2005, **4**,173.

[16] J M D Coey1, P Stamenov, R D Gunning, M Venkatesan and K Paul, New Journal of Physics 2010, **12**, 053025

[17] Boris B. Straumal, Svetlana G. Protasova, Andrei A. Mazilkin, Eberhard Goering, Gisela Schütz, Petr B. Straumal, and Brigitte Baretzky Beilstein, J. Nanotechnol. 2016, **7**, 1936.

[18] Thomas Tietze, Patrick Audehm, Yu–Chun Chen, Gisela Schu¨tz, Boris B. Straumal, Svetlana G. Protasova, Andrey A. Mazilkin, Petr B. Straumal, Thomas Prokscha, Hubertus Luetkens,Zaher Salman, Andreas Suter, Brigitte Baretzky, Karin Fink, Wolfgang Wenzel, Denis Danilov& Eberhard Goering, Scientific Reports 2015, **5**, 8871.

[19] Boris B. Straumal, Andrei A. Mazilkin, Svetlana G. Protasova, Ata A. Myatiev, Petr B. Straumal, Gisela Schütz, Peter A. van Aken, Eberhard Goering, and Brigitte Baretzky, Phys. Rev. B 2009, **79**, 205206.

[20] T.C. Damen, S.P.S. Porto, B.Tell, Phys. Rev.1966, **142**, 570.

[21] Y. Segawa, A. Ohtomo, M. Kawasaki, Z. K. Tang, P. Yu, and G. K. L. Wong, Phys. Status Solidi B 1997, **202**, 669..

[22] S. Lautenschlaeger, J. Sann, N. Volbers, and B. K. Meyer, A. Hoffmann, U. Haboeck, and M. R. Wagner, Phys. Rev. B 2008, **77**, 144108.

[23] R. Dimitrov, M. Murphy, J. Smart, W. Schaff, J. R. Shealy, L. F. Eastman, O. Ambacher, and M. Stutzmann, J. Appl. Phys. 2000, **87**, 3375.

[24] L. K. Li, M. J. Jurkovic, W. I. Wang, J. M. Van Hove, and P. P. Chow, Appl. Phys. Lett.2000, **76**,

1740.

[25] M.J. Ying, W. Cheng, X.X. Wang, B. Liao, X. Zhang Z.X. Mei, X.L. Du, S.M. Heald, H.J. Blythe, A.M. Fox, G.A. Gehring, Mater. Lett. 2015, **144**, 12.

[26] Y.B. Lu, Y. Dai, M. Guo, Y.Lin, B. B. Huang, Phys. Chem. Chem. Phys. 2013, **15**, 5208.

[27] Z. L. Liu, X. He, Z. X. Mei, H. L. Liang, L. Gu, X. F. Duan and X. L. Du, J. Phys. D: Appl. Phys. 2014, **47**,105303.

[28] X.W. Ke, F.K. Shan, Y.S. Park, Y.J. Wang, W.Z. Zhang, T.W. Kang, D.J. Fu, Surf. Coat. Technol. 2007, **201**,6797.

[29] F.J. Manjon, B. Mari, J. Serrano, A.H. Romero, J. Appl. Phys.2005, **97**, 053516.

[30] C. Bundesmann, N. Ashkenov, M. Schubert, D. Spemann, T. Butz, E.M. Kaidashev, M. Lorenz, M. Grundmann, Appl. Phys. Lett.2003, **83**, 1974.

[31] F. Reuss, C. Kirchner, Th. Gruber, R. Kling, S. Maschek, W. Limmer, A. Waag, and P. Ziemann, J. Appl. Phys. 2004, **95**, 3385.

[32] Prakash Chand, Anurag Gaur, Ashavani Kumar, Journal of Alloys and Compounds 2012, **539**, 174.

[33] Renu Kumari, Anshuman Sahai, Navendu Goswami, Progress in Natural Science: Materials International **2015, 25**,300.

[34] David Raymand, T. Jesper, Jacobsson, Kersti Hermansson and Tomas Edvinsson, the J. Phys. Chem. C, 2012, **116**, 6893.

[35] J. Serrano, F. J. Manjón, A. H. Romero, A. Ivanov, M. Cardona, R. Lauck, A. Bosak, and M. Krisch, Phys. Rev. B 2010, **81**, 174304.

[36] Qi Feng, Wala Dizayee, Xiaoli Li, David S Score1, James R Neal, Anthony J Behan, Abbas Mokhtari, Marzook S Alshammari, Mohammed S Al-Qahtani, Harry J Blythe, Roy W Chantrell, Steve M Heald, Xiao-Hong Xu, A Mark Fox and Gillian A Gehring, New J. Phys. 2016, **18**, 113040.

[37] T. K. Gupta and W. G. Carlson, J. Mater. Sci. 1987, **20**, 3487.

[38] T. K. Gupta, W. D. Straub, M. S. Ramanachalam, J. P. Schaffer, and A. Rohatgi, J. Appl. Phys. 1989, **66**, 6132.

[39] Sasikala Devi Assa Aravindh, Udo Schwingenschloegl, and Iman S Roqan, J. Chem. Phys. 2015, **143**, 224703.